

Structural and electrical properties of nano structure lead oxide

SK. KHADEER PASHA^a, K.CHIDAMBARAM^{a,*}, N. VIJAYAN^b, W. MADHURI^a

^a *Materials Physics Division, School of Advanced Sciences, VIT University, Vellore – 632014, Tamilnadu, India*

^b *National Physical Laboratory (CSIR), New Delhi –110012, India*

Lead oxide sample was prepared at low temperature by the solvo-thermal method. The lead oxide samples were characterized by X-ray diffraction (XRD), FT-IR and transmission electron spectroscopy (TEM) were employed to identify the structural phases, vibrational stretching frequencies and particle nature. X-ray diffraction studies indicate the formation of stable crystalline phase at 75 °C. Transmission electron microscopy and selected area electron diffraction analysis confirms the crystalline nanorods of lead oxide of size 15 – 30 nm. The results of dielectric measurements as a function of frequency, temperature and Cole - Cole plots are reported.

(Received December 19, 2011; accepted February 20, 2012)

Keywords: Lead Oxide, Chemical Synthesis, Dielectric properties, Electrical conductivity

1. Introduction

Lead Oxide (PbO), an important industrial material, has been widely applied in gas sensors, pigments and paints [1, 2]. PbO has two polymorphic forms and a wide band gap: red α - PbO, stable at low temperature, and yellow β - PbO, stable at high temperature [3]. Because of its applications, considerable progresses have been made on the synthesis of lead (II) monoxide polymorphs (α - PbO and β - PbO) over the years. Methods such as thermal evaporation [4], sputtering [5], pulsed laser deposition [6], chemical vapour deposition [7], sol-gel, precipitation, solvo-thermal and hydrothermal processes [8] have been adopted for the synthesis of PbO. Of the available methods, precipitation, hydrothermal and solvo-thermal methods have gained importance due to the fact that they are simple, employ low synthesis temperature and ensure pure single and multi products. Among them, solvothermal synthesis has been a major focus in the preparative investigations due to the advantages over other techniques, such as low-cost, mild temperature, potential controllability over size and morphology, which play key roles in tailoring the properties of nanomaterials. Under low temperature conditions, many starting materials can undergo quite unexpected reactions, which are often accompanied with the formation of nanoscopic morphologies that are not accessible by traditional routes. Lead (II) monoxide (PbO) is a photo active semiconducting metal oxide and has gained industrial importance due to its potent application in diversified fields. It plays a vital role in the formation of electrode active mass in lead acid batteries that are used in a variety of areas due to its high power density, wide application temperature range, complete recycling system and relatively low price [10]. Ma et al [11], Niasari et al [12] and Chen et al [13] prepared nanocrystalline PbO and PbO

nanocrystals via combination of precipitation and thermal decomposition route. Li et al. [14] prepared PbO with one step solid state reaction of Pb(II) compound with NaOH at room temperature but only α - PbO was obtained by the method. Despite the methods available in the literature for the preparation of PbO and nano PbO, finding an efficient method to produce PbO with size control and orientation by simple methods is still a challenge to material scientists today. Recently, the synthesis of PbO nano structures has gained importance owing to their unusual physicochemical properties leading to outstanding applications as humidity sensors [14].

Complex impedance spectroscopic technique is considered to be a promising non-destructive testing method for analyzing the electrical processes occurring in a compound on the application of a.c. signal as input perturbation. The output response of polycrystalline compound (when plotted in a complex plane) represents grain, grain boundary and electrode properties with different time constants leading to successive semicircles [15].

The mechanism of electrical conductivity in ion conducting solid is also an important problem. The conductivity is generally studied as a function of temperature, and it may also depend on structural changes in the material [16].

The aim of this paper is synthesis, electrical and dielectric properties and characterization of lead oxide. In the present paper, we report the results of X - ray diffraction, Fourier transmission infrared spectroscopy (FT-IR), Transmission electron microscopy (TEM) and impedance measurements of lead oxide. The temperature and frequency dependence of electrical conductivity and the dielectric properties of the sample are reported.

2. Material and methods

2.1 Reagents

All the chemicals used in the present work are of analytical grade obtained from SD fine chemicals, India. These chemicals are used without further purification and double distilled water is used throughout the experiment.

2.2 Experimental

The lead oxide was prepared by dissolving lead acetate in butanol at room temperature and stirred continuously until a clear transparent solution is obtained. The solution is then adjusted to pH 9 and stirred continuously at 75 °C for 10 hrs by adding 1N NaOH which results in the formation of a dense precipitate and this is thoroughly stirred using a magnetic stirrer for about 10 h at 75 °C. This precipitate is then filtered and washed with double distilled water followed by drying in a hot air oven at 75 °C to yield lead oxide which is labeled as PBB75. The annealed powders were grounded and made in the form of circular pellets of dimension 13mm diameter and 3 – 4 mm thickness using a hydraulic press at a pressure of 400 MPa for various measurements. The pellets were dried for 1hr and then heat treated at 100 °C for 30 min in a hot air oven.

2.3. Instrumentation

The structural studies were carried out using a Bruker D8 Advance X - ray diffractometer for 2θ values ranging from 10 to 70 in step size 0.02° and 2s counting time using Cu K α radiation at $\lambda = 0.154$ nm. The FTIR spectra was recorded using AVATAR-330 FTIR thermo nicolet spectrophotometer in the wavelength range 400 - 4000 cm⁻¹ by KBr pellet technique. Transmission electron microscope images were recorded using 200KV HRTEM, model: JEM-2011, Japan. The temperature dependence of dielectric constant, dielectric loss, Nyquist's diagram, electrical modulus and conductivity studies were measured in the frequency range 50Hz - 5MHz using HIOKI high tester LCR meter. Circular pellets of 13 mm diameter and 3 mm thickness were placed between the electrodes of LCR bridge, which acts as a parallel plate capacitor for electrical and dielectric measurements.

2.4 Dielectric studies

The dielectric constant is one of the basic electrical properties of solids. The measurement of dielectric constant and loss as a function of frequency and temperature is of interest both from theoretical point of view and from the applied aspects. Practically, the presence of a dielectric between the plates of a capacitor enhances the capacitance. Essentially, ϵ_r is the measure the polarization with external electric field [17].

The powder samples were made into pellets and silver paste was applied on either surface of the sample, which acts as an electrode. Temperature variation of dielectric

response was carried out at various frequencies ranging from 50Hz to 5MHz. A HIOKI meter was used to measure the dielectric constant. The capacitance (C_p) and conductance (G) of the sample was measured from LCR meter. These are used to calculate real and imaginary parts of the complex impedance using the standard relations [16].

$$Z^* = Z' + jZ'' = 1 / (G + j\omega C_p) \quad (1)$$

$$Z' = G / (G + j\omega C_p) \quad (2)$$

$$Z'' = \omega C_p / (G + j\omega C_p) \quad (3)$$

The conductance were determined from the semi-circular complex impedances (Z versus Z') plots by taking the value of intersection of the low frequency end of the semicircle on Z' axis. The conductivity (σ) for the sample was calculated using the expression

$$\sigma = G (d / A) \quad (4)$$

where d and A are the thickness and area of the sample respectively.

The real (ϵ') and imaginary (ϵ'') parts of the complex dielectric constant were calculated from the relations,

$$\epsilon' = C_p d / A \epsilon_0 \quad (5)$$

$$\epsilon'' = \sigma / \epsilon_0 \omega \quad (6)$$

where ϵ_0 is the permittivity of the free space.

The data were also analyzed for the electrical modulus formalism [17]. The real (M') and imaginary (M'') parts of the complex electrical modulus ($M^* = 1/\epsilon^*$) were obtained from (ϵ') and (ϵ'') values using the relations, The real (ϵ') and imaginary (ϵ'') parts of the complex dielectric constant were calculated from relations,

$$M' = \epsilon' / (\epsilon'^2 + \epsilon''^2) \quad (7)$$

$$M'' = \epsilon'' / (\epsilon'^2 + \epsilon''^2) \quad (8)$$

3. Results and discussion

3.1 Structural analysis

The XRD patterns of the as synthesized lead oxide sample at 75°C shown in Fig. 1. All the diffraction peaks corresponds to monoclinic Pb₂O₃ [JCPDS 76-1791], orthorhombic PbO [JCPDS 88-1589] and tetragonal Pb₃O₄ [JCPDS 88-1589]. The patterns implied that the material was composed of mixed phases.

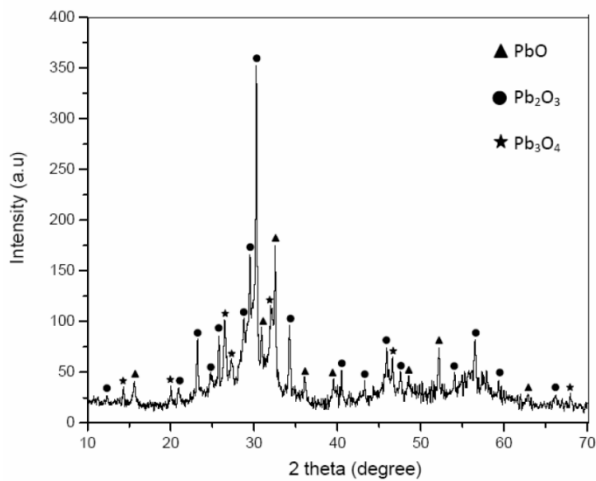


Fig.1. Room Temperature XRD Pattern of Mixed phase PbO.

3.2. FT-IR analysis

In Fig. 2. shows the FT-IR spectra of the sample lead oxide. The entire spectra exhibit a broad band centered around 3430 cm^{-1} which is ascribed to the -OH stretching vibration of water molecule. The appearance of the shoulder around 1630 cm^{-1} is attributed to the H-O-H bond bending vibrations. These vibrations arise due to the ability of the lead oxides to adsorb moisture from the surroundings during the sample preparation for the FT-IR analysis. The shoulder at 1400 cm^{-1} is due to the vibrations of strong bonding of oxygen with Pb. The band at 672 and 498 cm^{-1} is assigned to Pb-O bond vibrations [18].

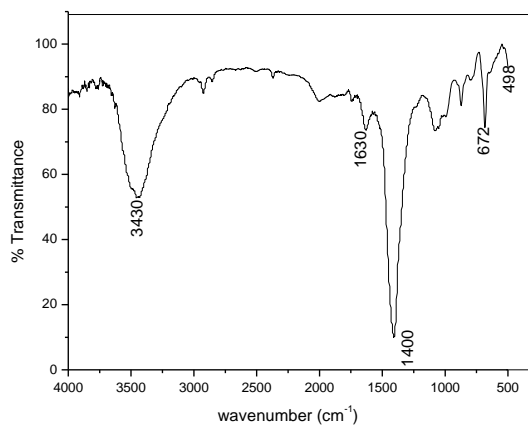


Fig. 2. Room Temperature FT-IR Pattern of mixed phase PbO.

3.3. Transmission electron microscopy

Transmission electron microscopy image of PBB 75 sample are shown in Fig. 3. The image indicates that the sample PBB 75 consists of multi nano rods and nanoparticles with diameter range of $15 - 30\text{ nm}$. The SAED pattern (Fig. 3 inset) indicates that the PbO nanocrystalline. It is confirmed by the X-ray diffraction analysis.

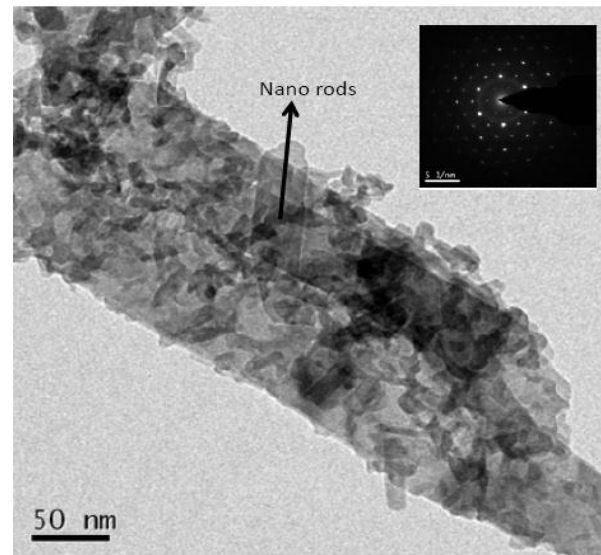


Fig. 3. TEM pattern of multi phase PbO and (inset) SAED.

3.4. Impedance analysis

The dielectric spectroscopy technique was used to analyze the electrical response of lead oxide in a wide range of frequency (50 Hz to 5 MHz) in the temperature range $25\text{--}250\text{ }^{\circ}\text{C}$. Fig. 4(a) and (b) shows the variation of the real part (Z') and imaginary part (Z'') of impedance with frequency (Nyquist's diagram) at different temperatures ($25\text{--}250\text{ }^{\circ}\text{C}$). It is observed that the magnitude of Z' decreases with the increase in both frequency as well as temperature indicating an increase in a.c. conductivity with the rise in temperature and frequency. Above 40 kHz Z' attains a constant value at all temperatures. This may be due to the release of space charges as a result of reduction in the barrier properties of material with the rise in temperature, and may be a responsible factor for the enhancement of a.c. conductivity of material with temperature at higher frequencies. Further, at low frequencies the value of Z' decreases with rise in temperature showing negative temperature coefficient of resistance (NTCR).

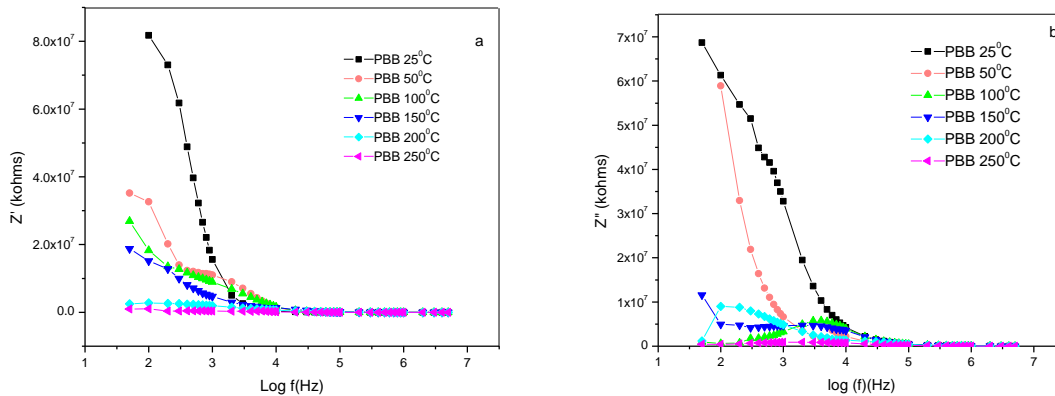


Fig. 4(a-b). Variation of (a) real part of complex impedance (Z') and (b) imaginary part of complex impedance (Z'') of mixed phase lead oxide with frequency.

The dielectric response has been examined by measuring both real and imaginary parts of the dielectric constants in the range of 50Hz to 5MHz. The variation of real (ϵ') and imaginary (ϵ'') parts of dielectric constant with frequency for lead oxide at different temperature is shown in Fig. 5(a-b). It is observed from the figures that the frequency increases the real and imaginary part of the dielectric constants decrease. This is due to the absence of dipolar relaxation process in the material. Semicircular arcs in the Cole – Cole plots observed in the high-frequency zone also confirms the absence of dipolar relaxation.

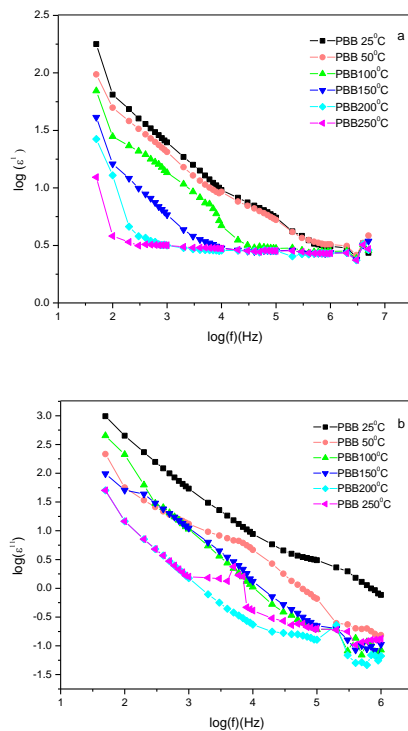


Fig.5. (a-b). Variation of real part of dielectric constant of lead oxide with frequency and (b) variation of imaginary part of dielectric constant of mixed phase lead oxide.

The dielectric loss also decreases with increasing frequency (Fig. 6) at different temperatures. It is observed that as the temperature increases the dielectric loss also increases at low frequencies.

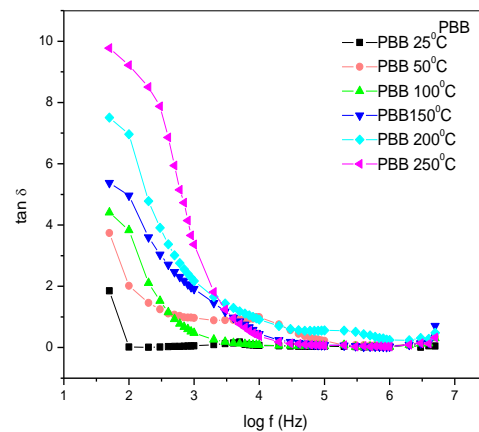


Fig. 6. Variation of dielectric loss with frequency at different temperatures.

The complex dielectric parameters were usually plotted in the complex plane represented by the real part versus imaginary part (Cole-Cole plot). Fig. 7 shows the experimental results of resistivity Cole - Cole plot of lead oxide at several temperatures. The behavior of the electrical response obeys the Cole – Cole formulae [19]. The impedance plot exhibits good semicircles. A typical impedance plot for mixed phase PbO at various temperatures is shown in Fig. 7. Some of the semicircles are incomplete especially at temperatures below 200 °C, since the resistivity of the sample is very large at low temperatures and the low-frequency end is limited by the measurement. As the temperature is raised, the semicircle becomes smaller and the variation appeared as an inclined spike (portion of the other semicircle) at the low frequency end. It indicates that the resistance of the sample decreases

with the increasing temperature and the mobile ion has surface electrode effect at higher- temperature regions.

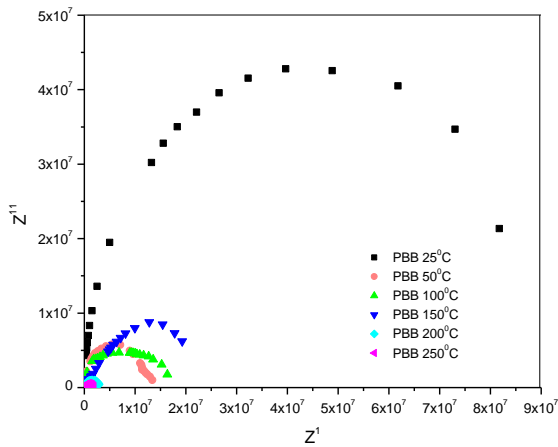


Fig. 7. Cole-Cole plots of mixed phase PbO at different temperature.

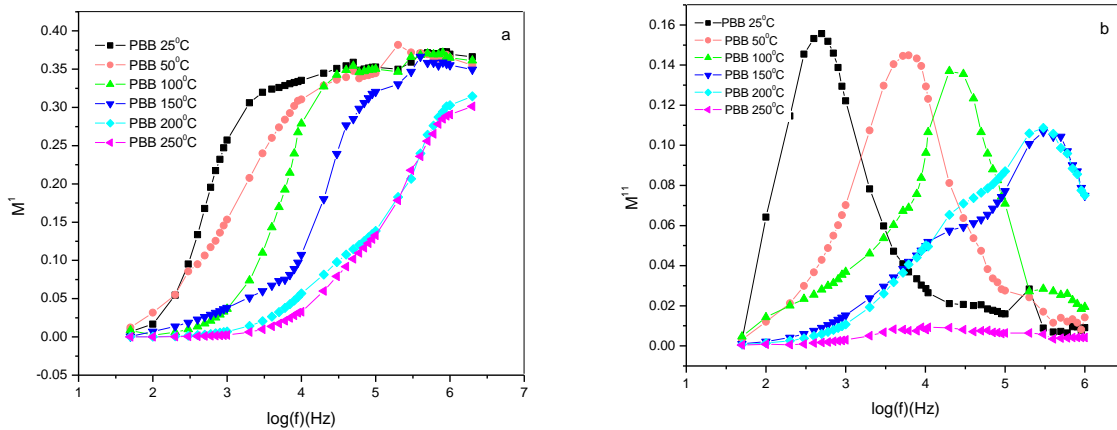


Fig. 8.(a-b). Variation of (a) real part (M') and (b) imaginary part (M'') of the dielectric modulus with frequency for mixed phase PbO at different temperatures.

3.5 Conductivity measurements

Electrical conductivity ($\sigma_{d.c}$) is a thermally activated process and follows the Arrhenius law. The d.c. conductivity evaluated from the impedance plots of PbO sample as a function of temperature are shown in Fig.9. Activation energy for conduction (E_a) of grains could be calculated from the slope of the straight line obtained from $\log \sigma_{d.c}$ versus T^{-1} . The corresponding values is same as calculated from modulus of oxygen vacancies, and are consistent with those obtained by the present impedance studies and also with earlier reports [20].

The plots of $\ln \sigma_{ac}$ Vs $1/T$ at various frequencies Fig. (10) show two different regions corresponding to high temperature intrinsic region and low temperature extrinsic

The DC conductivity of the sample was extracted from the Cole-Cole plot at zero frequency. The DC conductivity, $\sigma(0)$ is the reciprocal of the DC resistivity. It is in the order of $11.11 \times 10^{-9} \Omega^{-1} \text{cm}^{-1}$ at room temperature. It increases rapidly with increasing temperature. At 250 °C, the DC conductivity is $470.59 \times 10^{-9} \Omega^{-1} \text{cm}^{-1}$.

Variation of real (M') and imaginary (M'') parts of the electric modulus as a function of frequency at various temperatures have been shown in Fig.8. It is evident from Fig. 8 (a) that for each temperature, M' reaches a constant value at higher frequencies. Also, at lower frequencies, M' approaches to zero, confirming the presence of an appreciable electrode and/or ionic polarization in the temperature range studied. The value of M' increases from the low frequency towards a high frequency limit $1/\epsilon_\infty$ and the dispersion shifts to high frequency as temperature increases. The variation M'' with frequency at various temperatures is shown in Fig. 8(b). It is evident from the figure that the relaxation peaks shifts towards higher frequency with increase in temperature.

region. The activation energy can be calculated from the straight line region of the Arrhenius plot. The activation energies at various frequencies are tabulated, in Table.1. In the extrinsic region the conductivity can be mainly attributed to impurities. Upto 1MHz frequencies it is noticed that the band gap can be averaged to 0.36 eV. This value indicates that the conduction in the intrinsic region can be due to the e^- transition between $\text{Pb}^{2+} \leftrightarrow \text{Pb}^{3+}$ and $\text{Pb}^{3+} \leftrightarrow \text{Pb}^{4+}$ such a phase transition is also seen in the XRD pattern shown in Fig. 1.

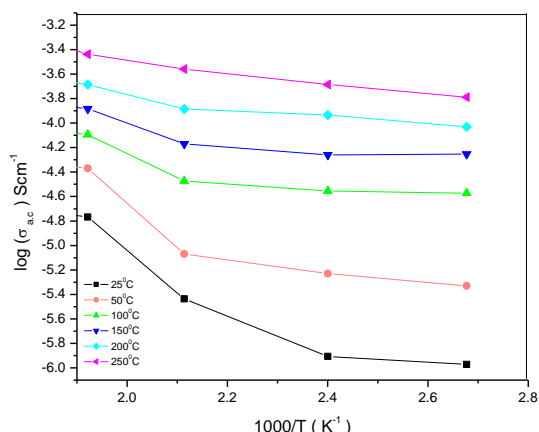


Fig. 10. Variation of $\sigma_{a.c.}$ versus $1000/T$.

Table 1. Activation energies of mixed phase lead oxide (PBB) from AC conductivity studies.

Frequency (Hz)	Band gap (eV) (PBB)
10Hz	0.403
10KHz	0.238
100KHz	0.349
1MHz	0.355
2MHz	0.207
3MHz	0.174
4MHz	0.157
5MHz	0.163

Table 2. Critical exponents from the variation of mixed phase lead oxide (PBB) from AC conductivity as a function of frequency.

Temperature (°C)	n_1	n_2
25	0.7103	0.3292
50	0.7597	0.3243
100	0.5626	0.2576
150	0.6761	0.2933
200	0.3774	-
250	0.2902	-

The plot between ac conductivity versus frequency is shown in Fig. (11). The ac conductivities exhibit a change of slope to higher values as the frequency is increased. It

shows a nearly flat portion at lower frequencies and increases to higher values of conductivity at higher temperatures. The linearity indicated that the contribution of ionic conduction is increasing as the temperature is raised. In analogy with Fig. (10) here also two regions are noticed. The frequency variation of ac conductivity can be fitted to the equation $\sigma(w) = \sigma_0 + Aw^{n_1} + Bw^{n_2}$ [21] where σ_0 is the contribution from dc electrical conductivity, A, B, n_1 and n_2 are factors of power law. The values of n_1 and n_2 calculated from the plots Fig. (11) are tabulated in Table 2. However in the extrinsic region the frequency dependence of ac conductivity can be fitted to a single power law as, $\sigma_w = \sigma_0 + Aw^{n_1}$ as the σ_0 values are in good agreement with the dc conductivity values calculated from Cole – Cole plots [16]. However the frequency response of ac conductivity can be interpreted in terms of hopping mechanism for n_1 and n_2 values ranging between $0 \leq n_1, n_2 \leq 1$ [21]. At high temperatures conduction is mainly due to the thermally activated hopping mechanism.

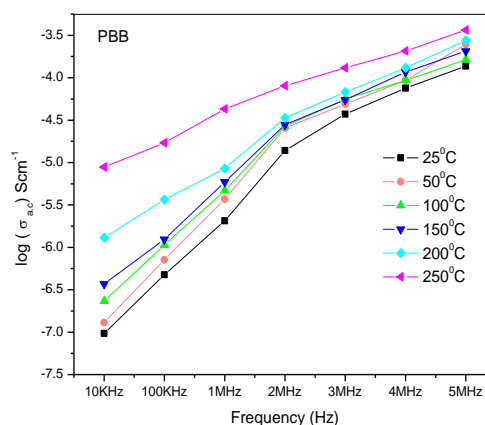


Fig. 11. Variation of $\sigma_{a.c.}$ versus frequency.

4. Conclusions

The Lead oxide samples were prepared at low temperature by the simple solvothermal method. Preliminary X-ray diffraction studies indicate the formation of stable phase at 75 °C. The conductivity studies of lead oxide sample have been carried out in a wide range of frequencies and temperatures. From the Cole - Cole plots the DC conductivity of both the samples was calculated at different temperatures and the real and imaginary parts of dielectric constants decreased with increase in frequency. The variation of d.c. conductivity (bulk) as a function of temperature demonstrates that the compound exhibits Arrhenius type of electrical conductivity. A hopping mechanism of electrical transport processes in the system is evident from the frequency analysis of $\sigma_{a.c.}$. It is concluded that, at low temperature it is possible to obtain stable, multiphase and high dielectric constant lead oxide with butanol as a solvent.

Acknowledgements

Authors gratefully acknowledge the Management of VIT University, Vellore for encouraging and providing necessary facilities for carrying out this work. The authors are thankful to Dr. S. Kalainathan, Department of Physics, VIT University, India, for providing the dielectric measurement facilities.

References

- [1] P. Veluchamy, M. Sharon, M. Shimizu, H. Minoura, *J. Electroanal. Chem.* **365**, 179, (1994).
- [2] S. Ghasemi, M.F. Mousavi, M. Shamsipur, H. Karami, *Ultrason. Sonochem.* **15**, 448, (2008).
- [3] L. Zhang, F. Guo, X. Liu, J. Cui, Y.T. Qian, *J. Cryst. Growth.* **280**, 575 (2005).
- [4] T. B. Light, J. M. Eldridge, J. W. Matthews, J. H. Greiner, *J. Appl. Phys.* **46**, 1489 (1975).
- [5] Y. Pauleau, E. Harry, *J. Vac. Sci. Technol. A.* **14**, 2006 (1996).
- [6] M. Baleva, V. Tuncheva, *J. Mater. Sci. Lett.* **13**, 4 (1994).
- [7] L. D. Madsen, *J. Am. Ceram. Soc.* **81**, 988 (1998).
- [8] Z. Liping, F. Guo, X. Liu, J. Cui, Y. Qian, *J. Cryst. Growth.* **280**, 575 (2005).
- [9] M. Shiota, T. Kameda, K. Matsui, N. Hirai, T. Tanaka, *J. Power Sources* **144**, 358 (2005).
- [10] F. G. Ma, Z. Q. Shao, L. Y. Song, H. M. Tan, *Hechenghuaxue* **9**, 449 (2001).
- [11] M. S. Niasari, F. Mohandes, F. Davar, *Polyhedron* **28**, 2267 (2009).
- [12] L. J. Chen, S. M Chang, Z. S. Wu, Z. J. Zhang, H. X. Dang, *Mater. Lett.* **59**, 3119 (2005).
- [13] J. Li, L.Y. Gong, X. Xia, *Yingyonghuaxue* **18**, 264 (2001).
- [14] Sk. Khadeer Pasha, K.Chidambaram, L. John Kennedy, J. Judith Vijaya, *Sensor and Transducers* **122**, 113 (2010).
- [15] P. S. Sahoo, A. Panigrahi, S. K. Patri, RNP Choudary *Bull. Mater. Sci.* **33**, 129 (2010).
- [16] V. C. Veeranna Gowda, R. V. Anavekar, *Solid state ionics* **176**, 1393 (2005).
- [17] S. Goma, C. M. Padma, C.K. Mahadevan, *Mater. Lett.* **60**, 3701 (2006).
- [18] V. Timar, R. L. Ciceo, I. Ardelean, *Semiconductor physics, Quant. Elect. and Optoelect.* **11**, 221 (2008).
- [19] S. Li, W. Yang, M. chen, J. Gao, J. Kang, Y. Qui, *Mat. Chem. Phy.* **90**, 262 (2005).
- [20] R. H. Chen, Chen-Chieh Yen, C. S. Shern, T. Fukami, *Solid State Ionics* **177**, 2857 (2006).
- [21] M. Pollak, T. H. Geballe, *Phys. Rev.* **122**, 1745 (1961).

*Corresponding author: kccb99@yahoo.co.in